Research Article | Vol. 25, No. 21 | 16 Oct 2017 | OPTICS EXPRESS 25407

Optics EXPRESS

Passive compensation of laser-induced higher-order aberrations in high-power NIR optics

MARTIN STUBENVOLL,* BERND SCHÄFER, AND KLAUS MANN

Laser-Laboratorium Göttingen, Hans-Adolf-Krebs-Weg 1, 37077 Göttingen, Germany
*Martin.Stubenvoll@llg-ev.de

Abstract: We report a method for passive compensation of thermally induced focal shifts and higher-order aberrations of NIR laser processing optics. Theoretical considerations are made on the elimination of aberrations including polarization effects using a multi-stage compensation element with optical flats of both positive and negative *dn*/*dT*. A compensation layout is designed and optimized utilizing numerical simulations of thermo-optic effects. Based on these findings, optical elements for compensation of an F-Theta objective are manufactured. By means of wavefront measurements and beam caustic measurements the feasibility of simultaneous passive compensation of focal shifts and higher-order aberrations is demonstrated.

OCIS codes: (220.1000) Aberration compensation; (140.6810) Thermal effects; (160.4670) Optical materials.

References and links

1. A. Kudryashov, V. Samarkin, A. Rukosuev, and A. Alexandrov, "High-power lasers and adaptive optics," Proc. SPIE **5333**, 45–52 (2004).
2. A. Kudryashov, V. Samarkin, A. Alexandrov, J. Sheldakova, and P. Romanov, "Wide aperture (more than 500 mm) deformable mirrors for high power laser beam correction," Proc. SPIE **8960**, 89601G (2014).
3. T. Graf and H. Hügel, *Laser in der Fertigung* (Vieweg + Teubner, 2009), Chap. 2.
4. J. Degallaix, C. Zhao, L. Ju, and D. Blair, "Simulation of bulk-absorption thermal lensing in transmissive optics of gravitational waves detectors," Appl. Phys. B **77**(4), 409–414 (2003).
5. J. Degallaix, C. Zhao, L. Ju, and D. Blair, "Thermal lensing compensation for AIGO high optical power test facility," Class. Quantum Gravity **21**(5), S903–S908 (2004).
6. J. Knittel, H. Richter, M. Hain, S. Somalingam, and T. Tschudi, "A temperature controlled liquid crystal lens for spherical aberration compensation," Microsyst. Technol. **13**(2), 161–164 (2006).
7. G. Eberle, V. Chiron, and K. Wegener, "Simulation and realization of a focus shifting unit using a tunable lens for 3D laser material processing," Phys. Procedia **41**, 441–447 (2013).
8. M. Blum, M. Büeler, C. Grätzel, and M. Aschwanden, "Compact optical design solutions using focus tunable lenses," Proc. SPIE **8167**, 81670W (2011).
9. Scanlab datasheet, "VarioSCAN, VarioSCAN$_{de}$i," http://www.scanlab.de/sites/default/files/pdf-dateien/data-sheets/varioscanvarioscande-en.pdf (2015).
10. M. Scaggs and G. Haas, "Thermal lensing compensation optic for high power lasers," Proc. SPIE **7913**, 79130C (2011).
11. S. Piehler, C. Thiel, A. Voss, M. Abdou Ahmed, and T. Graf, "Self-compensation of thermal lensing in optics for high-brightness solid-state lasers," Proc. SPIE **8239**, 82390Z (2012).
12. M. Stubenvoll, B. Schäfer, and K. Mann, "Measurement and compensation of laser-induced wavefront deformations and focal shifts in near IR optics," Opt. Express **22**(21), 25385–25396 (2014).
13. C. Thiel, M. Stubenvoll, B. Schäfer, and T. Krol, „Reliable Beam Positioning for Metal-based Additive Manufacturing by Means of Focal Shift Reduction," presented at the 2015 Lasers in Manufacturing Conference (LiM), Munich, Germany, 22–25 June 2015.
14. M. J. Weber, *Handbook of Optical Materials* (CRC, 2003).
15. Schott datasheet, "Optical Glass: Data Sheets," Schott North America Inc. (2013).
16. M. Stubenvoll, B. Schäfer, K. Mann, A. Walter, and L. Zittel, "Photothermal absorption measurements for improved thermal stability of high-power laser optics," Proc. SPIE **8885**, 88851R (2013).
17. J. C. Wyant and K. Creath, "Basic Wavefront Aberration Theory for Optical Metrology," in Applied Optics and Optical Engineering, Vol. XI, R. R. Shannon and J. C. Wyant, ed. (Academic, 1992).

#303704 https://doi.org/10.1364/OE.25.025407
Journal © 2017 Received 31 Jul 2017; revised 21 Sep 2017; accepted 23 Sep 2017; published 5 Oct 2017

Optics EXPRESS

1. Introduction

Due to the ongoing progress in the development of high power solid-state lasers and their application in a large number of fields in industry and science, beam line optics are required to guide and form beams of continuously increasing average powers and fluences. However, the advantages of these high power lasers can only be fully exploited if beam line optics and focusing objectives introduce merely negligible amounts of thermally induced wavefront aberrations. Thus, any substantial increase in brilliance requires careful observation of thermo-optic effects, such as focal shifts and higher-order aberrations, and, if necessary, their reduction or elimination. If a reduction of absorption alone does not yield the required results, compensation schemes may be considered.

Numerous compensation approaches are reported in literature, of which active compensation offers by far the greatest flexibility. Active compensation comprises e.g. the use of adaptive mirrors [1–3], heated compensation plates [4,5], as well as adaptive lenses which are controlled by heating of liquid crystal layers [6] or fluid pressure [7,8]. Finally, active compensation may be achieved by conventional lenses which are adjustable along the beam axis [9]. However, all these approaches require external control, either by an open-loop or by a closed-loop control system. In both cases a considerable amount of complexity is introduced into the optical system. Especially in an industrial production environment, where cost efficiency and reliability are essential, this is often undesirable. Furthermore, a simple, retrofittable solution may be helpful when facing unacceptable thermo-optic aberrations in existing optical systems.

Thus, passive compensation approaches can be taken into consideration as an alternative. Scaggs and Haas [10] have proposed an athermalized optical system using CaF_2 as lens material. Piehler et al. [11] present theoretical considerations on passive compensation of thermal effects induced by transient temperature distributions. In previous papers [12,13] a passive compensation scheme utilizing a single plane optical element with a negative thermo-optic coefficient dn/dT has been examined by the authors, yielding a reduction in focal shift of an industrial F-Theta objective by a factor of up to 2.5.

However, in the aforementioned publications the problem of stress-induced birefringence in the compensating element remained unconsidered, introducing astigmatism which leads to bifocusing of the laser beam. Moreover, a passive compensation scheme also for higher-order aberrations (e.g. spherical aberration) would be desirable. In this paper we further extend the passive compensation approach by introducing additional plane optical elements in front of an F-Theta objective. Thus, the challenge of passively compensating both higher-order aberrations and astigmatism associated with stress-induced birefringence can be tackled simultaneously.

2. Theory

In the following it is assumed that a circular and well collimated laser beam passes through an optical system of axial symmetry to be corrected. As compensation elements a number of K plane plates with thickness l_k is positioned in a row in front of this optics, thus introducing no net aberration in the low power limit. At least one of the plane elements needs to have a thermo-optic coefficient dn/dT opposite to the system to be corrected. The thermally induced wavefront aberrations of the optical system w_{opt} as well as those of the correcting elements w_k are assumed to be small enough so that the column approximation holds, and the total aberration w_{comp} may be approximated by summing up the individual contributions. Then, by expanding the individual terms as an M^{th}-order power series with respect to the radial coordinate r, the total aberration for the radial (superscript R) and tangential (superscript T) polarization obtained from K plane elements and the optics to be corrected can be written as

Optics EXPRESS

$$\begin{aligned} w_{\text{comp}}^{\text{R}}\left(r,l_k\right) &= \sum_{k=1}^{K}\sum_{m} w_{\text{k,m}}^{\text{R}}\left(l_k\right) r^{2m} + \sum_{m} w_{opt,\text{m}}^{\text{R}} r^{2m}. \\ w_{\text{comp}}^{\text{T}}\left(r,l_k\right) &= \sum_{k=1}^{K}\sum_{m} w_{\text{k,m}}^{\text{T}}\left(l_k\right) r^{2m} + \sum_{m} w_{opt,\text{m}}^{\text{T}} r^{2m} \end{aligned} \tag{1}$$

Equation (1) does not depend on an angular coordinate φ, since the geometry of the sample and the heating beam, as well as radial and tangential polarization states are rotationally symmetric.

Out of the large number of relevant parameters only the thickness dependence of the plane element coefficients has been emphasized in Eq. (1), as it is modified easiest and will thus serve as design variable in the following. After the different materials for the multiple-stage compensation have been selected, minimization of the average RMS-deformation

$$w_{\text{comp}}^{\text{RMS}}\left(l_1,\ldots,l_K\right) = \sqrt{w_{\text{comp}}^{\text{RMS,R}}\left(l_1,\ldots,l_K\right)^2/2 + w_{\text{comp}}^{\text{RMS,T}}\left(l_1,\ldots,l_K\right)^2/2} \tag{2}$$

with respect to l_i yields a non-linear system of equations, which may be solved numerically, once the thickness dependence of the w-coefficients in Eq. (1) is known. Hence, in order to compensate M radial terms in Eq. (1) at least $K = 2M$ elements are required for a complete determination of the expansion coefficients. However, the obtained solution will usually not be satisfactory in the presence of stress-birefringence because each term within the difference

$$\begin{aligned} \Delta w_{\text{comp}} &= w_{\text{comp}}^{\text{R}}\left(r\right) - w_{\text{comp}}^{\text{T}}\left(r\right) \\ &= \sum_{k=1}^{K} w_k^{\text{R}}\left(r\right) - w_k^{\text{T}}\left(r\right) + w_{\text{opt}}^{\text{R}}\left(r\right) - w_{\text{opt}}^{\text{T}}\left(r\right) \\ &= \sum_{k=1}^{K} \frac{n_k^3}{2}\left(B_{rrrr}^k + B_{rrtt}^k\right)\left(\sigma_{tt}^k - \sigma_{rr}^k\right) + \frac{n_{\text{opt}}^3}{2}\left(B_{rrrr}^{\text{opt}} + B_{rrtt}^{\text{opt}}\right)\left(\sigma_{tt}^{\text{opt}} - \sigma_{rr}^{\text{opt}}\right) \end{aligned} \tag{3}$$

turns out to be positive (n_k, n_{opt}: refractive indices of compensation elements and optics to be corrected; B_{rrrr}, B_{rrtt} and σ_{rr}, σ_{tt}: components of stress-optic tensor and radial and tangential stress components, integrated over element length, respectively). Since $\sigma_{tt} = \sigma_{rr}$ at the sample axis ($r = 0$) and $\sigma_{tt} > 0$, $\sigma_{rr} = 0$ (azimuthal tensile stress, force-free boundary, respectively) at the cylindrical surface, the difference $\sigma_{tt} - \sigma_{rr}$ is greater than or equal to zero. Due to the proportionality of the stress-optic components B to the elasto-optic coefficients (given e.g. in [14]) for isotropic materials, B_{rrrr} and B_{rrtt} are, for most optical glasses, positive. As a consequence Δw_{comp} increases monotonically with the number of elements required. However, if a rotation of the polarization state is performed after the K_1-th element in the compensation chain, instead of Eq. (3) one obtains the expression

$$\begin{aligned} \Delta w_{\text{comp}} &= \sum_{k=1}^{K_1} w_k^{\text{R}}\left(r\right) - w_k^{\text{T}}\left(r\right) + \sum_{k=K_1+1}^{K} w_k^{\text{T}}\left(r\right) - w_k^{\text{R}}\left(r\right) + w_{opt}^{\text{T}}\left(r\right) - w_{opt}^{\text{R}}\left(r\right) \\ &= \sum_{k=1}^{K_1} \frac{n_k^3}{2}\left(B_{rrrr}^k + B_{rrtt}^k\right)\left(\sigma_{tt}^k - \sigma_{rr}^k\right) - \sum_{k=K_1+1}^{K} \frac{n_k^3}{2}\left(B_{rrrr}^k + B_{rrtt}^k\right)\left(\sigma_{tt}^k - \sigma_{rr}^k\right) \\ &\quad - \frac{n_{\text{opt}}^3}{2}\left(B_{rrrr}^{\text{opt}} + B_{rrtt}^{\text{opt}}\right)\left(\sigma_{tt}^{\text{opt}} - \sigma_{rr}^{\text{opt}}\right) \end{aligned} \tag{4}$$

which may assume either positive or negative values, thus permitting a compensation of birefringence.

Figure 1 shows the complete scheme for a 2nd order compensation of aberrations and stress birefringence of a fused silica F-Theta objective as employed in the measurements, including four plane elements consisting of two compensating materials.

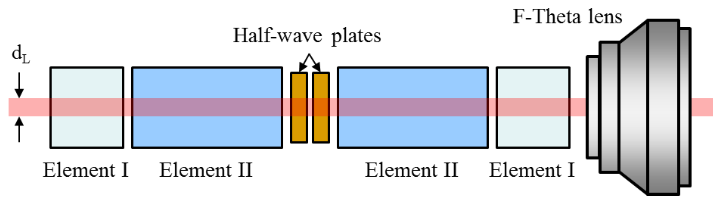

Fig. 1. Layout of a compensation scheme for focal shifts and higher-order aberrations of an F-Theta objective. The compensating elements are split into two symmetric sections with a 90° rotation of the polarization in between.

The required 90°-rotation of polarization is carried out by two λ/2 wave plates rotated by 45° against each other. Due to the fact that fused silica exhibits virtually no stress birefringence, the compensation chain may be arranged in mirror symmetry with respect to the half-wave plates.

For a more general and comprehensive theoretical treatment of thermo-optic effects, refer to Ref [12].

3. Numerical optimization

In order to implement a compensation layout with two different compensating materials, the two optical glasses BK7 ($dn/dT > 0$) and N-PK51 ($dn/dT < 0$) by Schott were chosen. For numerical optimization the wavefront deformations of the two materials induced by a collimated fundamental mode beam (P_L = 120 W, λ_L = 1070 nm, d_L = 6 mm, linear polarization) were simulated on a 35 × 35 mm^2 cross-section element for the thicknesses 3, 6, 12, 18, 25, 40 and 70 mm, using material parameters from [15]. Subsequently, polynomials of the form

$$w_{\parallel,\perp} = ar^6 + br^4 + cr^2 + d \tag{5}$$

were fitted to the central area along x and y cross sections of the simulated wavefront deformations, thus parallel and perpendicular to the initial polarization, on a radius of 3.5 mm (to take a slightly greater area than the 1/e^2 beam radius into account for parameterization). Figure 2 shows a simulated wavefront aberration for a 70 mm thick N-PK51 element, as well as polynomials fitted along the *x* and *y* axes in the central section. A deviation of the shapes due to stress birefringence can easily be recognized. Apart from the irrelevant constant *d*, the thickness dependence of coefficients *a*, *b* and *c* in Eq. (5), required for the minimization of Eq. (2), were then parameterized with equations of the form

$$a,b,c(l) = s_{a,b,c} \frac{p_{a,b,c} l + 1}{q_{a,b,c} l + 1} l. \tag{6}$$

The empirical formula Eq. (6) yields very good approximation results for the simulated coefficients and furthermore reflects the correct linear behavior in the plane stress and plane strain limits [12]. An exemplary course of the coefficient $a(l)$ is also given in the right part of Fig. 2 for both compensation materials.

Optics EXPRESS

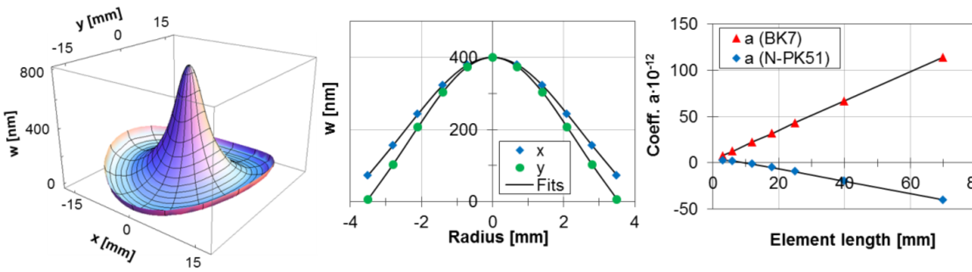

Fig. 2. Left: Simulated wavefront deformation induced by a laser beam (d_L = 6 mm, P_L = 120 W) in an N-PK51 sample of the dimensions 35 × 35 × 70 mm^3. Center: Polynomial fits in the central area of the simulated wavefront deformation in *x* and *y* directions on a diameter of 7 mm. Right: Parameterized coefficient *a* (cf. Equation (5)) by fitting Eq. (6) to thickness-dependent coefficients determined through numerical simulations.

Along with the simulation of the compensation elements, the thermal behavior of the F-Theta objective has to be calculated numerically. As only the thermally induced aberrations are of interest the individual lenses of the objective were approximated by plane fused silica elements of the respective center-thickness and taking into account the beam expansion inside the objective. The (relatively small) aberrations of the half-wave plates are simulated, too, and summed up with the contribution of the objective elements rescaled to the initial beam size. Equation (5) is subsequently fitted to this sum, representing the w_{opt} terms of Eq. (1). The model for the simulation of the objective and the half-wave plates is outlined in Fig. 3.

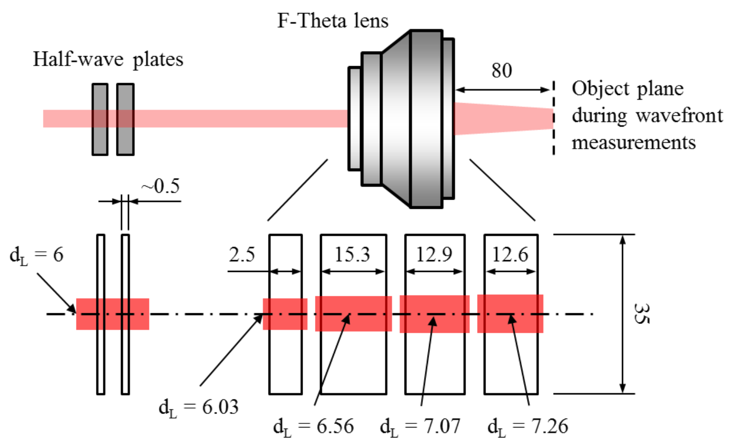

Fig. 3. Model for the simulation of thermo-optic aberrations within the half-wave plates and the individual fused silica lenses of an F-Theta objective approximated as plane elements (all dimensions in mm).

With all the thickness-dependent and polarization-dependent form functions known, one obtains

$$
\begin{aligned}
w_{\text{comp}}\left(r, l_{\text{NPK}}, l_{\text{BK}}\right) = \\
&\overbrace{\begin{matrix} w_{1,\|}^{\text{BK}}\left(l_{\text{BK}}\right) r^2 + w_{1,\|}^{\text{NPK}}\left(l_{\text{NPK}}\right) r^2 \\ + w_{2,\|}^{\text{BK}}\left(l_{\text{BK}}\right) r^4 + w_{2,\|}^{\text{NPK}}\left(l_{\text{NPK}}\right) r^4 \\ + w_{3,\|}^{\text{BK}}\left(l_{\text{BK}}\right) r^6 + w_{3,\|}^{NPK}\left(l_{\text{NPK}}\right) r^6 \end{matrix}}^{\text{before rotation of polarization}}
\overbrace{\begin{matrix} + w_{1,\perp}^{\text{BK}}\left(l_{\text{BK}}\right) r^2 + w_{1,\perp}^{\text{NPK}}\left(l_{\text{NPK}}\right) r^2 \\ + w_{2,\perp}^{\text{BK}}\left(l_{\text{BK}}\right) r^4 + w_{2,\perp}^{\text{NPK}}\left(l_{\text{NPK}}\right) r^4 \\ + w_{3,\perp}^{\text{BK}}\left(l_{\text{BK}}\right) r^6 + w_{3,\perp}^{\text{NPK}}\left(l_{\text{NPK}}\right) r^6 \end{matrix}}^{\text{after rotation of polarization}}
\overbrace{\begin{matrix} + w_1^{\text{obj}} r^2 \\ + w_2^{\text{obj}} r^4 \\ + w_3^{\text{obj}} r^6 \end{matrix}}^{\text{objective}}
\end{aligned} \tag{7}
$$

with three coefficients $w_{1\ldots3}$ and two compensating materials (BK7, N-PK51), and taking into account the directions of polarization (∥, ⊥). The indices in Eq. (7) are abbreviated for better readability, using "NPK" for N-PK51" and "BK" for "BK7". The RMS value of the compensated wavefront is minimized along the beam radius (r_L = 3 mm) according to

$$w_{\text{comp,RMS}} = \sqrt{\frac{1}{r_L} \cdot \int_0^{r_L} w_{\text{comp}} \left(r, l_{\text{NPK}}, l_{\text{BK}}\right)^2 \mathrm{d}r} \stackrel{!}{=} \min. \tag{8}$$

The minimized RMS values are displayed in Fig. 4 as a function of $l_{\text{N-PK51}}$ along with the corresponding length of BK7. The global minimum for the compensated system is attained at $l_{\text{N-PK51}}$ = 36.4 mm, requiring l_{BK7} = 11.8 mm.

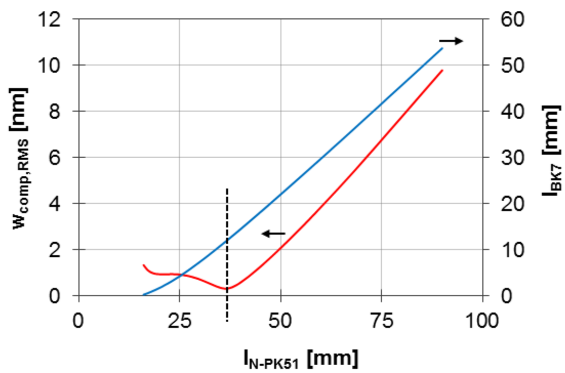

Fig. 4. RMS wavefront deformation of the entire compensation system minimized according to Eq. (8) with respect to $l_{\text{N-PK51}}$ (red) and corresponding thickness l_{BK7} (blue).

The simulated shape of the compensated wavefront is shown in Fig. 5 together with the simulated aberration induced by the F-Theta objective alone. As a consequence of the two-part design with a rotation of polarization, astigmatism caused by stress-induced birefringence is cancelled out and thermal effects are reduced by approximately an order of magnitude with only a very small amount of spherical aberration remaining.

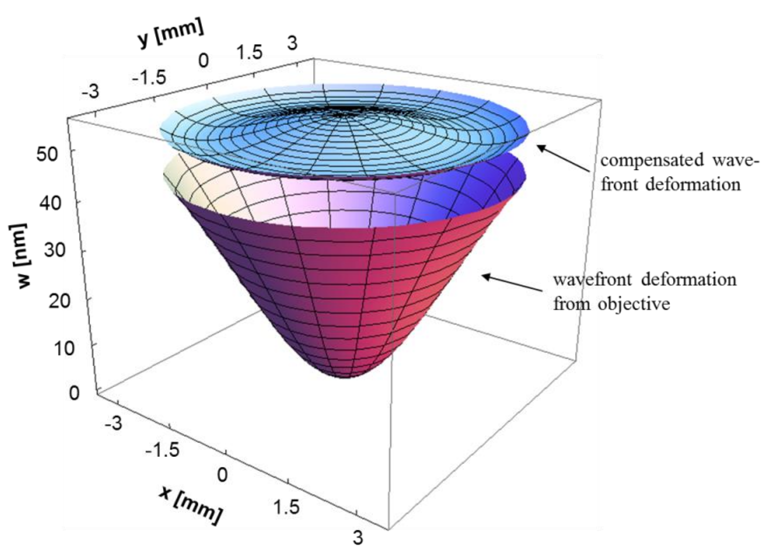

Fig. 5. Top: Simulated wavefront deformations (λ_L = 1070 nm, d_L = 6 mm, P_L = 120 W) of the F-Theta objective with optimized compensation system (w_{RMS} = 1.03 nm), as displayed in Fig. 1. Bottom: Simulated wavefront deformations of the uncompensated F-Theta objective for comparison (w_{RMS} = 12.82 nm).

Optics EXPRESS

4. Measurements of compensation system

Since the absorption coefficients used in the simulations are subject to production or batch variations, the samples for the experiments were fabricated with a certain safety margin in order to ensure that the negative *dn*/*dT* of N-PK51 suffices to compensate for the positive effects of the fused silica lenses. Therefore, the length for the N-PK51 samples was chosen to be 60 mm – somewhat away from the simulated optimum as in Fig. 4 – while the length of BK7 had to be shortened down to 9 mm following preliminary measurements. The reason for these deviations was merely the slightly higher absorption of BK7 and a considerably lower absorption of N-PK51 than measured in a preceding campaign [12,16]. All element surfaces facing laser radiation were anti-reflection (AR) coated.

4.1 Wavefront measurements

The experimental setup for the wavefront measurements utilizing a Hartmann-Shack sensor is outlined in Fig. 6. Primary attenuation is accomplished by using the reflected beam from two fused silica wedges aligned at their Brewster angle ($\theta_B \approx 56°$). In doing so, not only thermal effects from the attenuation are minimized due to the very low thermal expansion coefficient of fused quartz, but the attenuation is also polarization selective. This way, polarization effects can be investigated despite the statistically polarized nature of the 1070 nm Nd fiber laser. In order to further attenuate and adjust the beam power to the camera, a partially reflective (PR) mirror and several neutral density (ND) filters are used. The beam is imaged onto the sensor by a 4f configuration with a demagnification of 0.75. The object plane is located at the rear principal plane 80 mm behind the exit of the F-Theta objective. Two AR coated multi-order half-wave plates (Qioptiq) with a thickness of ~0.5 mm were used to rotate the polarization.

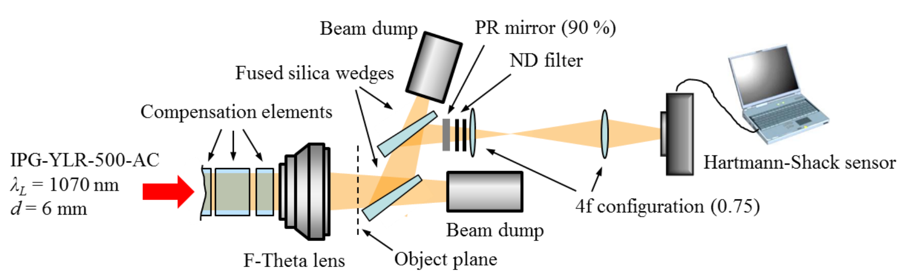

Fig. 6. Setup for wavefront measurements of the compensated/uncompensated F-Theta objective.

The very small thermally induced wavefront deformation quantities to be measured (a few tens of nanometers) require the elimination of effects (thermal and non-thermal) induced both by the beam delivery chain as well as the main defocus of the F-theta objective itself. Therefore, the reconstructed wavefront distributions were referenced to measurements of the F-theta objective without compensation elements installed. Furthermore, in the following only the most relevant effects, i.e. spherical aberrations and astigmatism induced by stress birefringence, are considered. Figure 7 shows the amount of wavefront aberration introduced by the compensation chain without (Fig. 7(a)) and with rotation of polarization (Fig. 7(b)) by means of two half-wave plates. The wavefront reconstruction shows only radial terms and primary astigmatism according to the “Arizona fringe” set of Zernike polynomials [17].

Optics EXPRESS

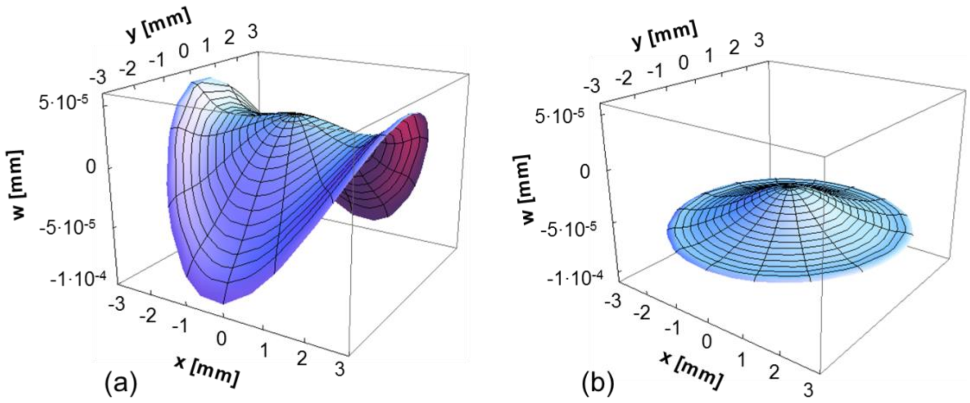

Fig. 7. Experimentally determined wavefront deformations plotted as differential images of measurements with and without compensation ($P_L \approx 75$ W, d_L = 6 mm, λ_L = 1070 nm). Wavefront (a) was captured without the two half-wave plates ($w_{RMS} = 3.23 \cdot 10^{-5}$ mm), while wavefront (b) was measured with the half-wave plates inserted ($w_{RMS} = 8.89 \cdot 10^{-6}$ mm).

While for the wavefront in Fig. 7(a) there is no useful compensation potential (astigmatic Zernike coefficient $C_4 = 3.5 \cdot 10^{-5}$), Fig. 7(b) shows high rotational symmetry due to the exploitation of polarization effects ($C_4 = 5.8 \cdot 10^{-7}$), proving the possibility of a complete cancellation of birefringence-induced astigmatism. Since the influence of the F-Theta objective has been subtracted, the displayed resulting wavefront can, in principle, be used for compensation. Since the wavefront has been optimized for higher-order compensation, its sign-reversed shape is supposed to correspond closely to a thermally induced wavefront deformation by the F-Theta objective.

4.2 Caustic measurements

As the relative nature of the wavefront measurements presented in the preceding section permits no prediction of the irradiance distributions in the vicinity of the beam waist, caustic measurements were conducted on the same experimental setup. The 4f configuration shown in Fig. 6 was therefore replaced by a camera on a linear stage.

The power-dependent measurements of the beam waist position, corrected for the additional focal shift introduced by the beam delivery chain, are shown in Fig. 8. For the uncompensated F-Theta objective the focal shift is positive and approximately linear with beam power. This behavior corresponds to an additional focusing of the beam. With four compensation elements (cf. Figure 1) inserted, a considerable astigmatism becomes apparent, corresponding to the astigmatic wavefront in Fig. 7(a). As a result, virtually no compensating power is delivered in x direction, while strong overcompensation occurs in y direction. If, finally, the two half-wave plates are inserted, the waist position remains close to the zero position for all powers with a relatively small deviation in x and y directions, indicating a substantial reduction of stress induced astigmatism. Again, this result is in good agreement with previous wavefront measurements (Fig. 7(b)). The reasons for the compensation potential being lower than predicted by simulation are mainly the residual non-corrected aberrations of the beam guidance optics preceding the actual setup, but also, to a lesser extent, imperfections from machining of the samples and possibly slight misalignments. However, the absolute average focal shift is reduced by a factor 2 to 5 for laser powers from 20 to 120 W, thus stabilizing the focal plane considerably and demonstrating at the same time an effective approach to compensating stress induced astigmatism and higher-order aberrations passively.

Optics EXPRESS

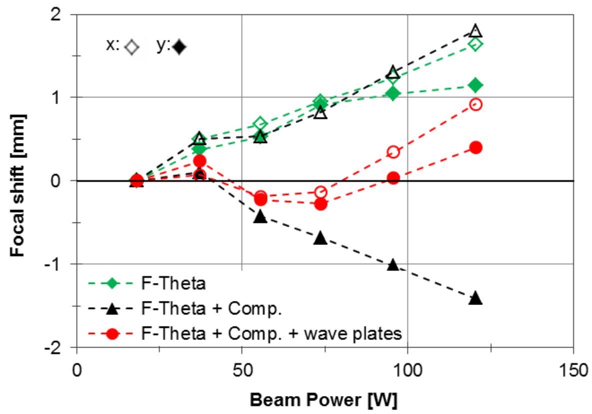

Fig. 8. Measured focal shifts of an F-Theta objective for x (hollow markers) and y (solid) directions using different compensation layouts.

5. Conclusion

In this paper an extension of a previously published passive compensation method for thermally induced wavefront aberrations [12] has been investigated, accomplishing also the compensation of higher order aberrations with a set of plane optical elements. To that end, the principle of a multiple-stage compensation scheme using different optical materials has been proposed, exploiting the deviating thermo-optic behaviors of different materials, each adding different – in sum compensating – terms to the aberrations of the overall system. Furthermore, astigmatism-inducing effects of stress birefringence were successfully canceled out by splitting the compensation layout into two sections and rotating the polarization of the beam by 90° in between.

The design of the compensation scheme was accompanied by thermo-optic simulations, taking into account both the (polarization-dependent) effects of the compensation elements and the objective to be compensated. Minimizing the thermally induced wavefront aberrations with respect to element thickness yielded an optimized sum of wavefront deformations from an F-theta objective and two compensating materials, which is an order of magnitude lower compared to the effects of the objective alone.

Subsequently, a compensation system for an F-Theta objective was implemented involving two sections of N-PK51 and BK7 plates with two multi-order half-wave plates among them to rotate the polarization. By means of wavefront measurements it could be proven that an effective compensation of stress birefringence is possible, and a rotationally symmetric wavefront can be provided to compensate the thermal effects of the focusing optics. With caustic measurements determining waist positions parallel and perpendicular to the polarization direction it could be shown that both astigmatism through thermally induced stress birefringence as well as focal shifts can be reduced considerably. Thus, the proposed multi-stage scheme opens a way for passive compensation of both first and higher order thermal aberrations in the sub-kW range of laser powers.

Acknowledgments

The authors would like to thank K. Hentschel and M. Zenz at Sill Optics GmbH for providing us with F-Theta objectives as test pieces as well as ray tracing results for the beam diameters inside the objectives and for straightforward help with AR coatings.